frontiers in
MICROBIOLOGY

ORIGINAL RESEARCH ARTICLE
published: 26 March 2012
doi: 10.3389/fmicb.2012.00109

Microbial iron cycling in acidic geothermal springs of Yellowstone National Park: integrating molecular surveys, geochemical processes, and isolation of novel Fe-active microorganisms

Mark A. Kozubal[1,2], Richard E. Macur[1,2], Zackary J. Jay[1,2], Jacob P. Beam[1,2], Stephanie A. Malfatti[3], Susannah G. Tringe[3], Benjamin D. Kocar[4], Thomas Borch[5] and William P. Inskeep[1,2]*

[1] *Thermal Biology Institute, Montana State University, Bozeman, MT, USA*
[2] *Department of Land Resources and Environmental Sciences, Montana State University, Bozeman, MT, USA*
[3] *Department of Energy–Joint Genome Institute, Walnut Creek, CA, USA*
[4] *Stanford Synchrotron Radiation Lightsource, Stanford, CA, USA*
[5] *Department of Soil and Crop Sciences, Colorado State University, Fort Collins, CO, USA*

Edited by:
Eric Roden, University of Wisconsin–Madison, USA

Reviewed by:
Vernon Phoenix, University of Glasgow, UK
Johannes Gescher, Karlsruhe Institute of Technology, Germany
David Barrie Johnson, Bangor University, UK

****Correspondence:***
William P. Inskeep, Department of Land Resources and Environmental Sciences, Montana State University, P.O. Box 173120, Bozeman, MT 59717, USA.
e-mail: binskeep@montana.edu

Geochemical, molecular, and physiological analyses of microbial isolates were combined to study the geomicrobiology of acidic iron oxide mats in Yellowstone National Park. Nineteen sampling locations from 11 geothermal springs were studied ranging in temperature from 53 to 88˚C and pH 2.4 to 3.6. All iron oxide mats exhibited high diversity of crenarchaeal sequences from the Sulfolobales, Thermoproteales, and Desulfurococcales. The predominant Sulfolobales sequences were highly similar to *Metallosphaera yellowstonensis* str. MK1, previously isolated from one of these sites. Other groups of archaea were consistently associated with different types of iron oxide mats, including undescribed members of the phyla Thaumarchaeota and Euryarchaeota. Bacterial sequences were dominated by relatives of *Hydrogenobaculum* spp. above 65–70˚C, but increased in diversity below 60˚C. Cultivation of relevant iron-oxidizing and iron-reducing microbial isolates included *Sulfolobus* str. MK3, *Sulfobacillus* str. MK2, *Acidicaldus* str. MK6, and a new candidate genus in the Sulfolobales referred to as Sulfolobales str. MK5. Strains MK3 and MK5 are capable of oxidizing ferrous iron autotrophically, while strain MK2 oxidizes iron mixotrophically. Similar rates of iron oxidation were measured for *M. yellowstonensis* str. MK1 and Sulfolobales str. MK5. Biomineralized phases of ferric iron varied among cultures and field sites, and included ferric oxyhydroxides, K-jarosite, goethite, hematite, and scorodite depending on geochemical conditions. Strains MK5 and MK6 are capable of reducing ferric iron under anaerobic conditions with complex carbon sources. The combination of geochemical and molecular data as well as physiological observations of isolates suggests that the community structure of acidic Fe mats is linked with Fe cycling across temperatures ranging from 53 to 88˚C.

Keywords: iron oxidation, iron reduction, ferric iron mat, geothermal, archaea, Sulfolobales, exobiology, jarosite

INTRODUCTION

Ferric iron oxyhydroxide and jarositic microbial mats are found in numerous environments and have been well studied in acid-mine-drainage systems such as Iron Mountain, CA, USA (Edwards et al., 1999; Singer et al., 2008) where Fe(II) and H_2SO_4 are produced during the oxidation of sulfide minerals such as pyrite and chalcopyrite (Nordstrom and Southam, 1997; Rohwerder et al., 2003). The phylogenetic diversity of microbial populations in acidic systems has been reviewed and acidophiles that respire on Fe(III) have been identified in various mesophilic systems (Blake and Johnson, 2000; Hallberg and Johnson, 2001; Baker and Banfield, 2003; Johnson and Hallberg, 2009). Microbial populations and description of novel species from thermo-acidophilic, iron-rich environments have also been studied (Johnson et al., 2003, 2006; Macur et al., 2004; Inskeep et al., 2005, 2010; Kozubal et al., 2008). Ferric iron mats from acidic geothermal springs in Yellowstone National Park (YNP) provide an outstanding natural laboratory to study thermophilic microorganisms that utilize ferrous iron for energy acquisition coupled to CO_2 fixation as their primary carbon source. Their ability to thrive in high-temperature environments with minimal requirements other than CO_2 and inorganic constituents suggests that these organisms are important primary producers in acidic high-temperature environments. However, the limited energy available from the oxidation of Fe(II) results in the formation of copious amounts of iron oxides. It has been estimated that at pH 2, ∼120 mol of Fe(II) must be oxidized for the formation of 1 mol of glucose (Konhauser, 2007). Thus, low cell numbers can result in the oxidation of large amounts of iron,

which has implications in understanding the biomineralization of iron in many environments outside YNP, as well as throughout Earth's evolutionary history (e.g., banded iron formations; Konhauser, 1998; Kappler and Straub, 2005).

Rates of abiotic Fe(II)-oxidation are slow at pH values less than 4.5 [1×10^{-7} mol Fe(II) min^{-1}; Singer and Stumm, 1970]; therefore, acidophilic microbes have an advantage over neutrophiles by not having to compete for rapid abiotic oxidation of Fe(II). Biologically oxidized Fe(II) often accumulates as ferric oxide minerals, which range in thickness and hardness depending on the geochemistry, flow rate, and microbial populations present (Konhauser, 1998; Inskeep et al., 2004). Solid phase geochemical analyses have been conducted on several ferric iron mats in YNP including 2–4 cm thick amorphous Fe-oxide mats from an acid-sulfate-chloride (ASC) spring (pH ∼3) in the Norris Geyser Basin (NGB) region as well as more crystalline ferric oxides (i.e., goethite, hematite) and jarosite from an acid-sulfate (AS) system located at the Rainbow Springs region (Inskeep et al., 2005). However, new results from synchrotron Fe-extended-X-ray absorption fine-structure spectroscopy (EXAFS) and X-ray diffraction (XRD) analyses across a greater number of Fe-oxide mats are presented in the current study and integrated with aqueous geochemical data and microbial community structure to understand factors controlling Fe-biomineralization across different acidic high-temperature environments.

Previous work has also described the microbial diversity in several low pH, iron-rich geothermal springs in the NGB, Joseph's Coat Hot Springs, and Rainbow Hot Springs regions of YNP (Jackson et al., 2001; Inskeep et al., 2004, 2005; Macur et al., 2004). However, these studies were based primarily on a relatively small number of shorter-length 16S rRNA gene sequences from a few sampling locations. Therefore, a primary aim of this study is to present more comprehensive data on the microbial diversity from numerous acidophilic ferric mats in YNP over a wide variety of environmental conditions ($T = 53$–$88^{\circ}C$; pH = 2.4–3.6), including a larger library of 16S rRNA gene sequences obtained from "next-generation" pyrotag and community shotgun sequencing efforts.

Phylogenetic similarity of observed sequences from molecular studies to cultivated microorganisms (16S rRNA gene) is not sufficient to definitively link microbial metabolism(s) to specific geochemical cycles especially when 16S rRNA gene sequences are highly divergent from those of cultured organisms (e.g., <90% similarity). Therefore, the cultivation of relevant organisms from these habitats is also critical for implicating specific microorganisms and their corresponding metabolic pathways in biogeochemical processes. For example, we recently reported the isolation of a new Sulfolobales isolate from YNP ferric iron mats, *Metallosphaera yellowstonensis* str. MK1, an iron and sulfur-oxidizing chemolithoautotroph (Kozubal et al., 2008). Quantitative analysis of *Metallosphaera*-like 16S rRNA sequences demonstrated that organisms highly similar (>99%) to strain MK1 comprised up to 80% of the total archaeal community in various YNP ferric iron habitats.

The geothermal springs discussed in this study are highly reduced at the source and Fe(II)-oxidizing microbial communities do not occur until the springs have sufficient dissolved oxygen from atmospheric mixing, after dissolved sulfide has degassed. Previous quantitative expression results show that the *M. yellowstonensis foxA-J* gene cluster is important for Fe(II) oxidation in pure culture and *in situ* (Kozubal et al., 2011). The *fox* gene cluster is found in all iron-oxidizing Crenarchaeota (i.e., *Sulfolobus metallicus, Sulfolobus tokodaii,* and *Metallosphaera* spp.) and potential mechanisms for Fe(II) oxidation via Fox proteins have been hypothesized (Kozubal et al., 2011). It is not currently known how widespread this gene complex may be in other members of the Sulfolobales found in Fe-oxide mats, and/or in other archaea.

The primary goal of this study was to couple geochemical processes with microbial community analysis to understand mechanisms of Fe(II)-oxidation and secondary solid phase formation in acidic outflow channels of YNP geothermal springs. The specific objectives were to (i) determine *in situ* Fe(II) oxidation rates and identify predominant secondary minerals formed across a range of environmental conditions ($T = 53$–$88^{\circ}C$; pH = 2.4–3.6), (ii) identify the predominant community members of different high-temperature ferric iron microbial mats, (iii) characterize novel Fe-active isolates determined to be relevant *in situ* populations using molecular surveys, and (iv) present genomic evidence for iron and sulfur oxidation in a novel Sulfolobales isolate (strain MK5), as well as from site metagenomes.

MATERIALS AND METHODS

DESCRIPTION OF SITES

Eleven geothermal springs in Yellowstone National Park were chosen for this study and include eight acid-sulfate-chloride springs (ASC) in NGB, and three acid-sulfate springs (AS) springs from Joseph's Coat and Rainbow Springs (**Figure 1**). Each spring was sampled at multiple locations based on transects established within the main flow channel as a function of distance (temperature) from the outflow source (selected sites shown in **Figure 2**). The ASC springs sampled include "*OSP Spring*" (NGB-OSP), "*Beowulf Spring*" (NGB-BE, NGB-BW), "*Gap Spring*" (NGB-GAP), *Echinus Geyser* (NGB-EG), *Whirligig Geyser* (NGB-WG), "*Grendel Spring*" (NGB-GRN), and "*Porcelain Basin*" (NGB-PB; names in quotations are not official YNP names). Acid-sulfate springs included an unnamed spring at Joseph's Coat Hot Springs (JC2) and two unnamed springs at Rainbow Springs (RS2 and RS3).

DNA EXTRACTION AND 16S rRNA SEQUENCING

The distribution and relative abundance of total archaeal and bacterial 16S rRNA gene sequences were examined using microbial mat samples obtained with sterile tools and collection tubes and immediately placed on dry ice for transport to a −80°C freezer. Samples were obtained over a 5-year period from July 2003 to July 2008. Total DNA was extracted from field samples (or pure cultures) using a FastDNA SPIN kit for soil (Q-Biogene, Irvine, CA, USA). The nearly full-length 16S rRNA gene PCR primers included the *Bacteria*-specific primer Bac8f (5′-AGAGTTTGATCCTGGCTCAG-3′) coupled with the universal primerUniv1392r (5′-ACGGGCGGTGTGTAC-3′) and the *Archaea*-specific primer Arc2f (5′-TTCCGGTTGATCCYGCCGGA-3′) also coupled with the universal primer Univ1392r. Briefly, each

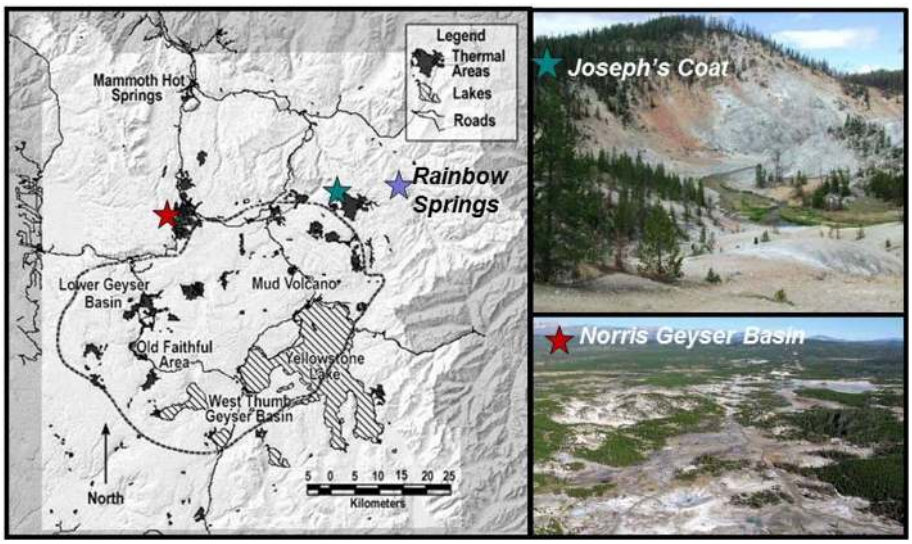

FIGURE 1 | Map of Yellowstone National Park indicating sampling locations at Rainbow Springs, Joseph's Coat Hot Springs, and Norris Geyser Basin (NGB).

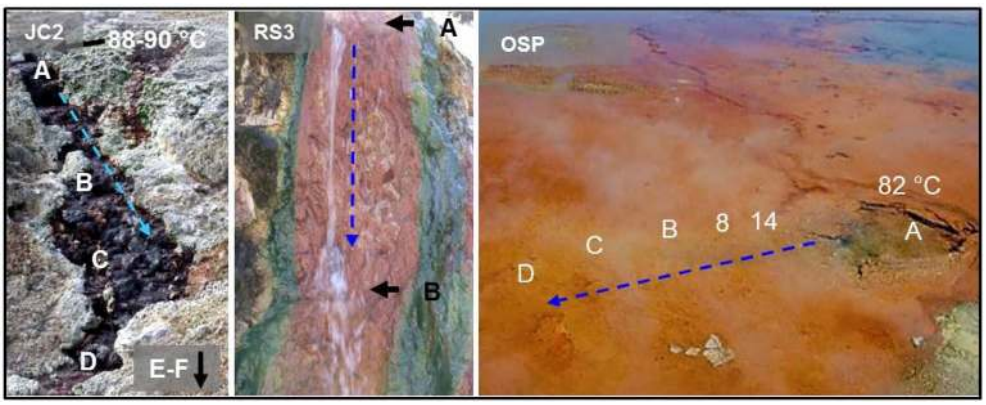

FIGURE 2 | Representative springs (JC2, RS3, and OSP) from Yellowstone National Park showing sampling points within the main flow channels, source water temperatures, and direction of flow channel (blue arrow).

50-μL PCR mixture contained 10 mM Tris–HCl (pH 8), 50 mM KCl, 0.1% Triton X-100, 4.0 mM $MgCl_2$, each deoxynucleoside triphosphate at a concentration of 800 μM, 0.5 μL of each primer, 1.25 U of *Taq* DNA polymerase (Promega, Madison, WI, USA), and 1–5 μL of template DNA (2–20 ng). The thermal cycler protocol was 94°C for 6 min, 25–35 cycles of 94°C for 45 s, 54°C for45 s, and 72°C for 110 s, and a final 7-min extension at 72°C. Negative control reactions (no template) were routinely performed to ensure purity. The purified PCR products were cloned using the pGEM-T vector system from Promega Corp. (Madison, WI, USA), and the inserts were amplified and sequenced (TGEN, Phoenix, AZ, USA, and the Ohio State Plant Genomics Facility, Columbus, OH, USA).

In addition to clone sequences obtained from the method described above, a total of 1348 near full-length 16S rRNA gene sequences were obtained from the Joint Genome Institute (JGI) for two Fe samples from OSP springs as part of a different metagenome study (Community Sequencing Project 787081). The primers used by JGI were *Bacteria* specific 27F (5′-AGAGTTTGATCCTGGCTCAG-3′) and 1391R (5′-GACGGGCRGTGWGTRCA-3′), and *Archaea*-specific 4aF (5′-TCCGGTTGATCCTGCCRG-3′) and 1391R (for details see http://www.jgi.doe.gov/sequencing/protocols/index.html). Finally, samples from several Fe mats (obtained in 2009) were used for 454 "pyrotag" sequencing (16S rRNA amplified template) at the DOE–JGI, including sampling locations at OSPB ($n = 31{,}237$), OSPC ($n = 8719$), OSPD ($n = 146$), BEE ($n = 3574$), and GRN ($n = 21{,}401$). The V6–V8 region of 16S rRNA was amplified using primers 926F (5′-cctatcccctgtgtgccttgg cag tct cag AAA CTY AAA KGA ATT GRC GG-3′) and 1392R (5′-ccatct cat ccc tgcgtgtctccg act cag ACG GGC GGT GTG TRC-3′). Primer sequences were modified by the addition of 454 A or B adapter sequences (lower

case). In addition, the reverse primer included a 5-bp barcode for multiplexing of samples during sequencing. Twenty-microliter PCR reactions were performed in duplicate and pooled to minimize PCR bias using 0.4 μL Advantage GC 2 Polymerase Mix (Advantage-2 GC PCR Kit, Clonetech), 4 μL 5X GC PCR buffer, 2 μL 5 M GC Melt Solution, 0.4 μL 10 mM dNTP mix (MBI Fermentas), 1.0 μL of each 25 nM primer, and 10 ng sample DNA. The thermal cycler protocol was 95°C for 3 min, 25 cycles of 95°C for 30 s, 50°C for45 s, and 68°C for 90 s, and a final 10-min extension at 68°C. PCR Amplicons were purified using SPRI Beads and quantified using a Qubit fluorometer (Invitrogen). Samples were diluted to 10 ng/μL and mixed in equal concentrations. Emulsion PCR and sequencing of the PCR amplicons were performed following the Roche 454 GS FLX Titanium technology manufacturer's instructions. Sequencing tags were analyzed using the software tool PyroTagger (http://pyrotagger.jgi-psf.org) using a 180-bp sequence length threshold as described in Engelbrektson et al. (2010). The 97% operational taxonomic units (OTUs) were also taxonomically classified by Blastn against a curated database of >1500 full-length 16S rRNA sequences from the actual sites that exhibited high nucleotide similarity (>96% of reads were 99.5% similar to prior long-fragment sequences).

CULTIVATION OF MICROORGANISMS FROM Fe MICROBIAL MATS

Approximately 2 g of Fe-oxide microbial mat from NGB-BE, NGB-GAPA, and NB-OSPB was placed into 60 mL serum bottles with synthetic growth medium as described by Kozubal et al. (2008) at sampling times between August 2003 and August 2008. Isolation of *Sulfobacillus* str. MK2 colonies was obtained by streaking ∼0.5 mL of NGB-BE slurry on 1.5% agar plates in synthetic media with 0.5% yeast extract and 10 mM $FeSO_4$. Plates were incubated at 58°C for up to 12 days. Colonies were transferred to serum bottle cultures with 10 mM $FeSO_4$, 0.2% YE in synthetic media for further study. Pure cultures of *Acidicaldus* str. MK6 and Sulfolobales sp. strain MK5 were obtained by streaking ∼0.5 mL of OSPB slurry on 1.2% Gelrite® plates in media described by Itoh et al. (2001) with 2 mM $FeSO_4$. Plates were incubated at 65°C for up to 15 days. Pure colonies of *Acidicaldus* str. MK6 were transferred to serum bottle cultures with synthetic media and 0.05% YE for further studies. *Sulfolobus* str. MK3 was obtained by dilution to extinction with 2% pyrite in synthetic media by the method described for *Metallosphaera* str. MK1 (Kozubal et al., 2008), except inoculum was obtained from GAPA and cultures were incubated at 75°C. The progress of all cultures was monitored by extracting DNA from the serum bottles, followed by PCR amplification of 16S rRNA genes using universal bacterial and archaeal primers and separation and visualization of the PCR products using denaturing gradient gel electrophoresis (DGGE; Macur et al., 2004). The purity of cultures was also confirmed by cloning and sequencing of near full-length16S rRNA gene fragments.

PHYLOGENETIC ANALYSES

Near full-length 16S rRNA gene sequences obtained from cloning were compared to sequences in public databases using the "Blastn" algorithm. Sequence alignments were performed using ClustalX (Version 1.83) and phylogenetic trees were constructed using the Maximum Likelihood method (MEGA 5.0) with 1000 boot straps (Tamura et al., 2011). Accession numbers for all 16S rRNA gene sequences discussed in the current study were deposited with NCBI [*Sulfobacillus* str. MK2 (DQ350778), *Sulfolobus* str. MK3 (JN944177), Sulfolobales str. MK5 (JN971012), and *Acidicaldus* str. MK6 (JQ247723)].

ISOLATE GROWTH CHARACTERISTICS

Temperature and pH optima were determined for all isolates in 20 mL serum bottles with 5 mL headspace composed of 30% O_2, 50% CO_2, and 20% N_2. Heterotrophic growth was determined with the addition of 0.5% yeast extract (YE); autotrophic growth with either 2% pyrite, 2% S^0, or 5 mM $Fe(II)SO_4$ without added carbon; and mixotrophic growth with 5 mM $Fe(II)SO_4$ and 0.5% YE. Anaerobic growth was evaluated using Fe(III) as a primary electron acceptor in 20 mL serum bottles with 15 mL of synthetic media, 0.5 g of dried, double-autoclaved NGB-BE mat (120°C), 10 mM glucose, and 0.5% YE. Serum bottle cultures were sealed and purged with N_2 gas for 20 min to obtain sub-oxic conditions.

IRON OXIDATION AND REDUCTION RATES

Iron oxidation rates were determined for *Metallosphaera* str. MK1 and Sulfolobales str. MK5 in 120 mL serum bottles with 1 g of crushed and dried, triple autoclaved NGB-BE HFO mat and 60 mL of BED synthetic media with 10 mM $FeSO_4$ without added carbon and a headspace composed of 50% O_2 and 50% CO_2. Oxidation rates of Fe(II) were determined with an initial cell culture of $\sim 10^6$ cells/mL added at exponential growth phase. Abiotic Fe(II)-oxidation rates were determined with un-inoculated controls. Fe(II) was measured on 1 mL filtered (0.2 micron filters) samples using the ferrozine method (To et al., 1999) on late exponential/lag phase cultures after the addition of 10 mM Fe(II). Samples were taken every 10 min for four hours after cell culture density reached 10^8 cells/mL. Culture density was measured by counting SYBR gold staining. Rates were reported as femtomoles Fe(II) per liter per second per cell after correcting for abiotic oxidation [0.025 μmol Fe(II) L^{-1} s^{-1}].

Iron reduction rates were determined for *Acidicaldus* str. MK6 and Sulfolobales str. MK5 in 120 mL serum bottles with 80 mL of synthetic medium, 10 mM glucose as the electron donor and 1-g triple autoclaved Fe(III)-oxide mat from NGB-BE, which has been previously characterized (Inskeep et al., 2004). Serum bottles were purged with N_2(g) for 20 min prior to inoculation. Samples were inoculated to an initial concentration of 10^5 cells/mL and 1 mL filtered samples were taken twice daily for 10 days and analyzed for Fe(II) as stated above. Cell concentrations were determined by SYBR gold staining and reduction rates were calculated on late exponential/lag phase cultures after cell culture densities reached 10^8 cells/mL and reported as femtomoles Fe(III) per liter per second per cell [abiotic Fe(III)-reduction rates were negligible].

SOLID PHASE CHEMICAL ANALYSIS

Solid phase analysis was performed on field samples and secondary phases obtained from *Metallosphaera* str. MK1 and Sulfolobales str. MK5 culture vessels after 11 days of incubation in *Beowulf* spring water and 2% ground pyrite at 65°C and pH 3.0. Strain MK1

culture vessels contained two distinct iron oxide phases including a dark-red phase around the glass vessel at the air/water interface and an off-yellow phase forming just below the air-water interface. Approximately 0.5–1 g of each phase was scraped from the bottles and analyzed by XRD or X-ray absorption spectroscopy (XAS).

Iron EXAFS spectra were collected at beamline 11-2 at the Stanford Synchrotron Radiation Lightsource. A double crystal Si(220) monochromator was used for energy selection. Scans were conducted from 100 eV below to 1000 eV above the Fe-K-edge at 7111 eV. Iron fluorescence spectra were averaged and normalized to unity using the XAS data reduction software SIXPACK (Webb, 2011). SIXPACK/IFEFFIT algorithms were used to isolate backscattering contributions by subtracting a spline function from the EXAFS data region. The resulting function was then converted from units of eV to $Å^{-1}$, weighted by k3, and windowed from 3 to 14 $Å^{-1}$ Linear combination of model compounds was performed to reconstruct unknown spectra; no more than four standards were varied at a time. Model compound (standards) contributions were deemed significant if their mole percentage was greater than 10%. Model compounds used for linear combination Fe-EXAFS fitting included two-line ferrihydrite sorbed to quartz sand, Si-substituted ferrihydrite, six-line ferrihydrite, lepidocrocite, goethite, hematite, potassium-jarosite, scorodite, synthetic and natural siderite, vivianite, magnetite, green rust phases (chloride, sulfate, carbonate), and amorphous FeS. Synchrotron X-ray powder diffraction was performed at 12,735 eV at beamline 11-3 (SSRL), with an energy resolution ($\Delta E/E$) of $\sim 5 \times 10^{-4}$ equipped with a Si(311) monochromator and a MAR345 CCD detector. Finely crushed samples were placed between two polycarbonate windows to a nominal thickness of 100 μm and mounted in an aluminum sample holder. Patterns were energy calibrated using a lanthanum hexaboride standard. Resulting powder diffraction images were radially integrated, converted to d-space vs. relative intensity, and analyzed for mineral phases using JADE 6.0 (Materials Data, Inc.).

MICROSCOPY

Optical images were obtained utilizing a Zeiss epifluorescence microscope (Zeiss Axioskop 2 plus; Zeiss, Oberkochen, Germany). Samples were stained with 10X SYBR-green for fluorescent images. Environmental samples for scanning electron microscopy (SEM) images were stored at 4°C prior to analysis. Samples were analyzed with either a SEM with cryostage or a field emission-scanning electron microscope (FE-SEM), both equipped with an energy-dispersive X-ray spectrometer (EDS) for elemental analysis.

RESULTS

GEOCHEMISTRY OF ACIDIC Fe-OXIDIZING SPRINGS IN YNP

The major electron donors, pH, oxygen concentration, temperature, and solid phase geochemistry of three acid-sulfate (AS; JC2, RS2, RS3) and eight acid-sulfate-chloride (ASC) geothermal springs (NGB-OSP, NGB-BE, NGB-BW, NGB-GAP, NGB-WG, NGB-EG, NGB-PB, NGB-GRN) are summarized across a total of 19 sampling positions (**Table 1**). The common geochemical properties across this group of thermophilic sites include pH (2.4–3.6), ferrous Fe (~30–240 μM), and dissolved oxygen (20–100 μM). The concentrations of other reduced constituents including arsenite, ammonium, dissolved hydrogen, and dissolved methane can be significant; however, the dissolved sulfide levels of Fe-oxide depositional zones are generally <5–10 μM. Although the concentrations of ammonium (NH_4^+) are ~20–30 times higher in AS springs compared to ASC springs, no consistent changes in NH_4^+ were observed as a function of distance from the spring source, regardless of total NH_4 concentration. Ferrous Fe represents the majority of total dissolved Fe at the point of discharge for nearly all springs sampled. Moreover, total soluble Fe did not decline significantly with distance (in some cases Fe_{TS} can decrease by 10–20%), indicating that the deposition rates of secondary Fe(III) phases are considerably slower than the total flux of Fe(II). However, the amount of ferrous Fe decreased substantially in acid-sulfate springs [JC2, RS2; e.g., levels of Fe(II) decline from 81 to 34 μM in RS2] matching the production of soluble ferric Fe (**Figure 3**), whereas ferric Fe remained low in ASC springs containing high concentrations of arsenic (e.g., >20 μM).

The short residence times between sampling positions in JC2 and RS2 (e.g., JC2A to JC2D is 35 s), combined with the amount of Fe(II)-oxidized results in very high rate constants for the oxidation of Fe(II) (**Figure 3**). A second spring source emerges at sampling position JC2E where Fe(II) is reset to near 100% of the total dissolved iron, and ~43% is oxidized to Fe(III) by sampling point JC2F, a 32-s residence time. Measurements of channel velocities and estimates of total flow rate were used to approximate *in situ* iron oxidation rates in outflow channels of JC2 and RS2. The average rates of Fe(II) oxidized within JC2, RS2, and BE Springs ranged from 0.5 to 1.3, 0.2 to 2, and 0.1 to 0.2 μM Fe(II) oxidized/second, respectively (**Figure 3**).

Solid phase analysis was completed for iron oxide mat samples from all sites discussed in the current study except *Grendel* Spring (**Table 1**; **Figure 4**). XRD and SEM/EDAX data from *OSP* Spring and *Whirligig* Geyser in NGB are similar to those found previously from *Beowulf* Spring (Inskeep et al., 2004) and show high levels of arsenate sorbed to amorphous ferrihydrite-like phases (As:Fe = 0.6–0.7). Solid phases from *Echinus* Geyser (**Figure 4**) are characterized by more crystalline ferrihydrite phase with lower sorbed arsenate, which is not surprising given the lower arsenic concentrations (**Table 1**). Scorodite ($Fe^{III}AsO_4 \cdot 2H_2O$) was the dominant phase detected using XRD in the higher temperature (85°C) Fe mats of *Porcelain Basin* and to a lesser extent in *GAP* Spring.

The lower pH acid-sulfate systems (e.g., JC2, RS2) contain higher concentrations of Fe(II), but lower levels of arsenic (**Table 1**). Solid phase analyses (XRD, XAS) indicate more crystalline phases including jarosite [$KFe_3(OH)_6(SO_4)_2$], goethite, and hematite within the outflow channels of RS2 and JC2, respectively (**Table 1**; **Figure 4**). These systems contain higher concentrations of sulfate, potassium, and total soluble Fe than sites in NGB and as a result, jarosite is an important phase formed in these environments. Jarosite contains Fe(III), and requires that Fe(II) be oxidized (Kappler and Straub, 2005). The abiotic rate of Fe oxidation is quite slow at low pH (Singer and Stumm, 1970), so biological mechanisms are likely responsible for the majority of

Table 1 | A geochemical summary of acid-sulfate-chloride springs (Norris Geyser Basin) and acid-sulfate springs (Joseph's Coat and Rainbow Springs) showing concentrations of major electron donors, O_2 and solid phase analysis using synchrotron X-ray diffraction.

Spring ID[1]	Sampling Point (m)[2]	T (C°)	pH	H_2S μM	O_2 μM	Fe^{II} μM	As^{III} μM	NH_4^+ mM	SO_4^{2-} mM	H_2 (aq) nM	Summary of SEM/EDAX and XRD analysis[3]
NGB-BE	A (0)	75	3.1	120	<3	36	26	0.066	1.5	60	Positions A–C: S^0
	D (6)	66	3	8	55	34	22	0.067	1.6	14	Positions D, E: ∼1–3 cm, soft
	E (7.5)	62	3	3	77	31	19	0.068	1.6	14	Amorphous Fe-oxyhydroxide; 0.7 mol As^V/mole Fe*
NGB-BW	A (0)	72	3	130	<3	33	24	0.067	1.6	40	Positions: A–C: S^0
	D(8.4)	60	3	2	87	30	18	0.068	1.6	11	Position D: ∼0.2–0.4 cm soft, Amorphous Fe-oxyhydroxide; 0.7 molAs^V/mole Fe*
NGB-OSP	A (0)	82	3.6	11	7	28	20	0.08	1.1	46	Positions B, C: ∼1–2 cm, soft
	B (2–3)[4]	73	3.5	2	31	27	21	0.079	1	46	amorphous Fe-oxyhydroxide; 0.6 molAs^V/mole Fe
	C (3.5)	65	3.5	<0.3	46	22	19	0.07	1	18	
	D (4)	57	3.5	<0.3	90	20	nd	0.08	1.1	nd	
NGB-GAP	A (0)	84	3.3	8	<3	63	25	0.065	1	148	Position B: 1–3 cm, soft
	B (0.3)	77	3.3	2	35	58	22	0.067	1	18	Scorodite
NGB-WG	A (0)	64	3.3	<0.3	nd	7	29	0.074	1.2	37	Edge of source pool: 1 cm, soft Amorphous Fe-oxyhydroxide
NGB-PB	A (0)	85	3.4	1.3	nd	13	29	0.068	1.1	12	Edge of source pool: 2–3 cm, soft Scorodite
NGB-EG	A (0)	76	3.5	3.5	44	37	3	0.066	3.2	120	Position C: 1–2 cm, soft
	C (10)	70	3.4	<0.3	56	35.5	2	0.069	3.2	99	Ferrihydrite
JC2	A (0)	88	2.6	4	<3	91	0.25	1.93	5.6	166	Position B, C, D: 0.2–0.4 cm, hard
	B (2.7)	75	2.5	<0.3	6	86	0.13	2.22	6	132	Goethite, hematite, quartz
	C (7.1)	65	2.4	<0.3	48	66	0.09	2.44	6.4	126	
	D (12)	59	2.4	<0.3	78	50	0.03	2.37	6.6	43	
	E (18.5)[5]	75	2.5	230	<3	88	0.33	2.42	5.9	126	Position E: S^0
	F (22.0)	56	2.4	30	48	72	0.19	2.47	6.3	41	
RS2	A (0)	77	2.6	7	<3	91	3.1	1.72	7.3	53	Position B, C, D: 0.2–0.4 cm, hard
	B (2.2)	73	2.5	2	22	81	2.5	1.74	7.3	32	K-jarosite, goethite, quartz
	C (2.3)[5]	77	2.7	6	<3	86	3	1.72	7.3	52	
	D (8.3)	69	2.6	1	44	76	2.5	1.76	7.5	37	
	F (12.6)	54	2.5	<0.3	99	34	0.9	1.75	7.4	28	
RS3	A (0)	54	3.2	<0.3	<3	220	1.1	1.47	6.3	27	Position A, B: 2–4 cm, soft
	B (0.9)	53	3.2	<0.3	14	200	1.2	1.47	6.3	17	Goethite, ferrihydrite

Mineralogy data from Beowulf Spring from Inskeep et al. (2004); all other sites from this study.

[1] *Spring abbreviations: NGB, Norris Geyser Basin, JC, Joseph's Coat Hot Springs; RS, Rainbow Springs (also see materials and Methods for different springs).*

[2] *Letters correspond to different sampling positions within the primary flow channel.*

[3] *SEM/EDAX, scanning electron microscopy–energy-dispersive analysis of X-rays: predominant locations and mat characteristics are provided.*

[4] *Sampling location of metagenome sample "OSP_8."*

nd, Not determined.

iron oxides and jarosite deposited in these systems. Furthermore, the log saturation indices for jarosite were calculated for RS2A, RS2C, and RS3A at −2.9, −1.2, and 0.3, respectively. Negative values indicate under-saturation of aqueous chemical species with respect to K-jarosite, indicating that these solutions would not be expected to precipitate jarosite, except perhaps in spring RS3. In contrast, saturation indices were greater than 10 for NGB-BE and NGB-OSP(owing primarily to the higher pH), which do not contain jarosite as a solid phase.

Solid phases of ferric iron observed using synchrotron XRD (major phases identified in **Table 1**) were used to constrain least squares fitting procedures of Fe-K-edge EXAFS spectra for all field samples. Least squares fits to experimental k3 weighted Fe-EXAFS spectra are shown for each of the major spring types studied here (**Figure 5**) and these fits provide further support for the predominant solid phases observed using XRD. Specifically, the ferric iron mats included in this study can be grouped into these main four categories based on mineralogy: high arsenate-amorphous Fe oxyhydroxides (sites BE, WG, OSP), ferrihydrite and/or scorodite (e.g., GAP, EG, PB), goethite and hematite (e.g., JC2), and jarositic systems containing less Fe oxide (e.g., RS2). The different phases of ferric Fe formed in these systems relate to differences in spring geochemistry and hydrodynamic properties. For example, arsenic concentrations are one to two orders of magnitude higher in NGB springs relative to RS2 and JC2, respectively, and may play an important role

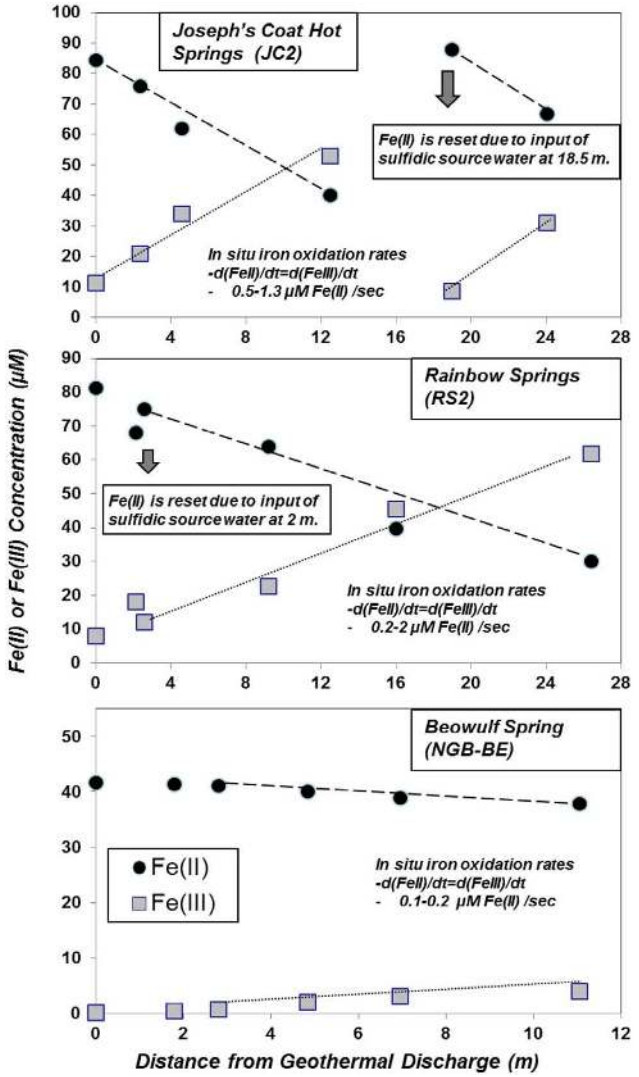

FIGURE 3 | Profile of Fe(II) oxidation in acidic geothermal springs at Joseph's Coat Hot Springs (JC2), Rainbow Springs (RS2) and Norris Geyser Basin (*Beowulf* Spring) plotted as the disappearance of Fe(II) or the production of Fe(III) as a function of time (or distance) within the outflow channel. The total soluble Fe at any position is the sum of Fe(II) and Fe(III), which agreed favorably (<10% difference) with total Fe determined using inductively coupled plasma spectrometry [ICP; total Fe values of JC2A, RS2A, and BEA are ∼100, 90, and 40 μM, respectively]. In JC2, ∼45% of the total ferrous Fe is oxidized to Fe(III) at sampling position D, corresponding to a 35-s travel time [sampling positions JC2E and RSC correspond to a second spring discharge, which resets the concentration of Fe(II)].

in the inhibition of jarosite precipitation and the subsequent formation of amorphous ferrihydrite phases containing significant amounts of sorbed arsenate (Inskeep et al., 2004). Also, the rate of amorphous ferrihydrite precipitation is faster than crystalline phases such as goethite, hematite and jarosite, and is consistent with the increase in dissolved Fe(III) from microbial ferrous iron oxidation in JC2 and RS2 relative to NGB-BE (**Figure 3**).

MICROBIAL COMMUNITY STRUCTURE

Molecular surveys of near full-length 16S rRNA genes present in acidic Fe mats reveal numerous different novel archaea, especially within the Crenarchaeota (i.e., orders Sulfolobales, Desulfurococcales, and Thermoproteales) as well as two deeply rooted novel lineages with no cultured relatives (referred to as "Novel Archaeal Groups" I and II; NAG1 and NAG2). All acidic Fe-oxide mats contained significant numbers of different Sulfolobales-like sequences, which clade with three of the known Sulfolobales genera; however, numerous entries cluster together within a previously undescribed lineage. Sequences related to the novel Sulfolobales clade are particularly well represented in NGB-WG and Joseph's Coat (Spring 2; **Figure 6**). An Fe(II)-oxidizing isolate was obtained representing this novel lineage (strain MK5), and is discussed in more detail below. The other Sulfolobales-like 16S rRNA gene sequences present across the acidic Fe mats include members of the *Metallosphaera* and *Sulfolobus* genera (**Figure 6**), and isolation of *M. yellowstonensis* from these sites was described in previous reports (Kozubal et al., 2008, 2011).

Sequences related to members of the candidate phylum Thaumarchaeota and Euryarchaeota were also observed in acidic Fe mats (**Figure 6**). Many of the thaumarchaeal sequences belong to a separate lineage compared to previously cultivated mesophilic isolates and the metagenome sequence from NGB-BE contains one scaffold over 1 Mb in length, which is discussed in detail elsewhere (Beam et al., 2011). The novel euryarchaeal sequences were observed in BE, OSP, and JC2, and are distantly related to *Thermoplasma volcanium* (∼89–90% similarity to 16S rRNA gene sequences in GenBank).

A significant majority (>99%) of bacterial 16S rRNA gene sequences obtained from acidic Fe mats above ∼70°C were related to *Hydrogenobaculum* spp., a deeply rooted member of the order Aquificales (**Figure 7**). However, bacterial diversity increased when temperatures decreased below 60–65°C. For example, bacteria distantly related to *Acidimicrobium*, *Acidovorax*, *Acidicaldus*, *Methylacidiphilum*, *Meiothermus*, *Geothermobacterium*, and *Sulfobacillus* spp. were found in greater abundance in down-gradient positions, depending on the specific spring. *Acidovorax*, *Acidicaldus*, and *Methylacidiphilum* spp. were more common in acid-sulfate springs (e.g., RS2EF), while *Meiothermus* and *Acidimicrobium*-like populations were observed with greater frequency in the acid-sulfate-chloride springs of NGB. Sequences related to *Acidicaldus*, *Geobacter*, and *Methylacidiphilum* spp. were especially important in Rainbow and Joseph's Coat channel positions below 55°C (e.g., 60–70% of PCR amplified long-fragment bacterial clones observed at RS3A, RS3B, and JC2C). Many of these bacterial sequences are highly divergent from cultivated relatives (<91% similarity, 16S rRNA gene), and include a novel clade related to *Geobacter* spp. (represented by sequences RS2F-SK964 and RS2F–SK975; **Figure 7**). The *Geobacter*-like sequences are only ∼83% (16S rRNA sequence similarity) related to the nearest cultivated delta-proteobacterium, *Geobacter uraniireducens*. Other noteworthy novel bacterial groups observed in these sites include sequences related to *Acidimicrobium ferrooxidans* (clone RS2F-SK971, 90%), *Sulfobacillus acidophilus* (RS2F-SK266, 89%), and finally, a distant relative of Heliobacteriaceae bacterium SLH (clone RS3B-SK292, 83%), representing a highly divergent sequence in the Firmicutes.

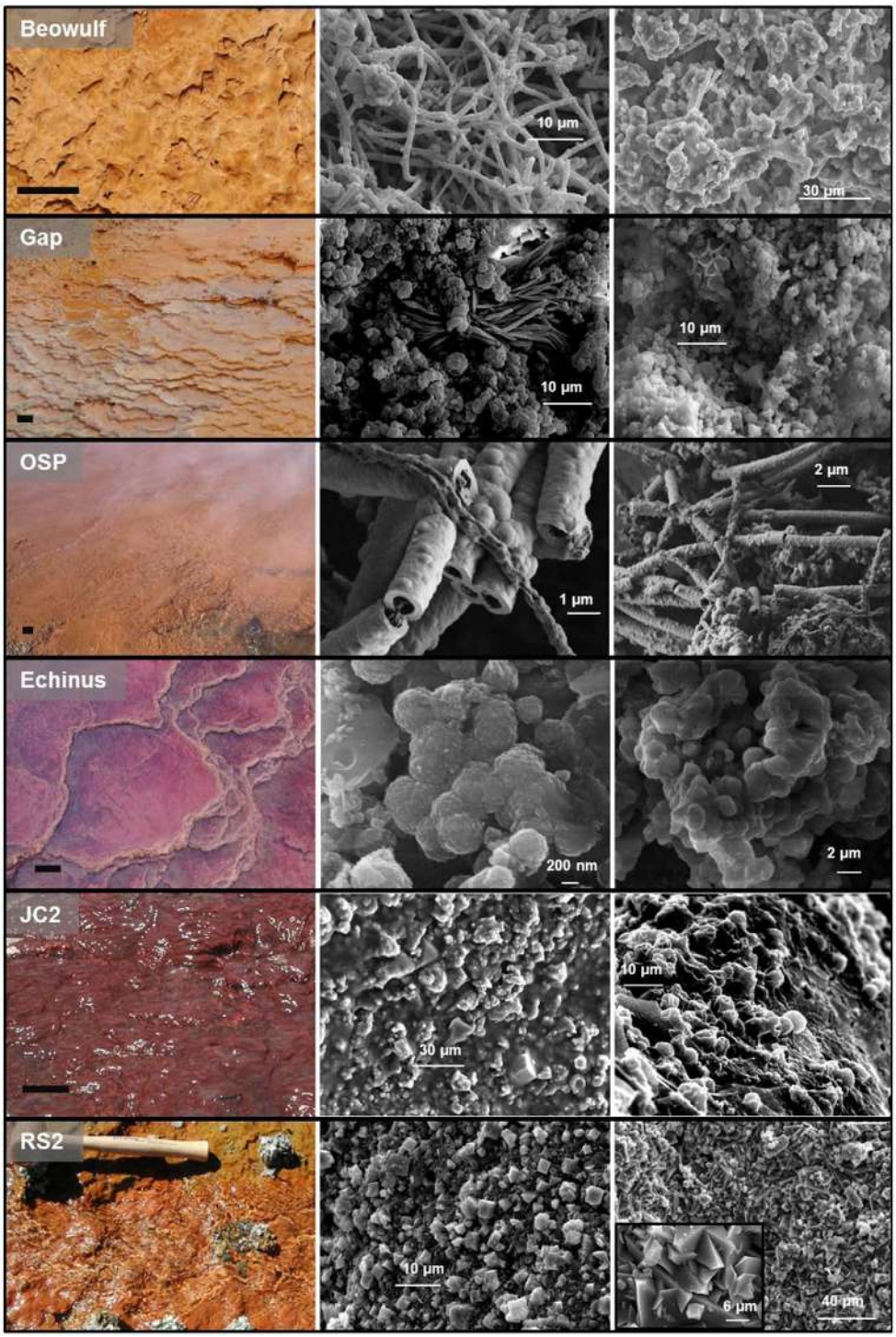

FIGURE 4 | Ferric iron phases from select ferric iron mats in Yellowstone National Park with corresponding scanning electron micrographs of solid phases found within each spring (results also presented in Table 1). Scale bar on site photographs is ∼5 cm.

DEEPER 16S rRNA GENE SURVEYS WITHIN OSP SPRING

Additional full-length 16S rRNA gene sequences (PCR clone libraries) were obtained at two locations within the outflow channel (pH 3.5) of OSP Spring (NGB) as part of a JGI ribosomal panel study of YNP geothermal systems (CSP 787081). The distribution of long-fragment 16S rRNA gene sequences observed in this dataset ($n \sim 1200$) shows extensive archaeal diversity in moderately oxygenated Fe mats NGB-OSP8 (72°C Fe mat) as well as 74°C

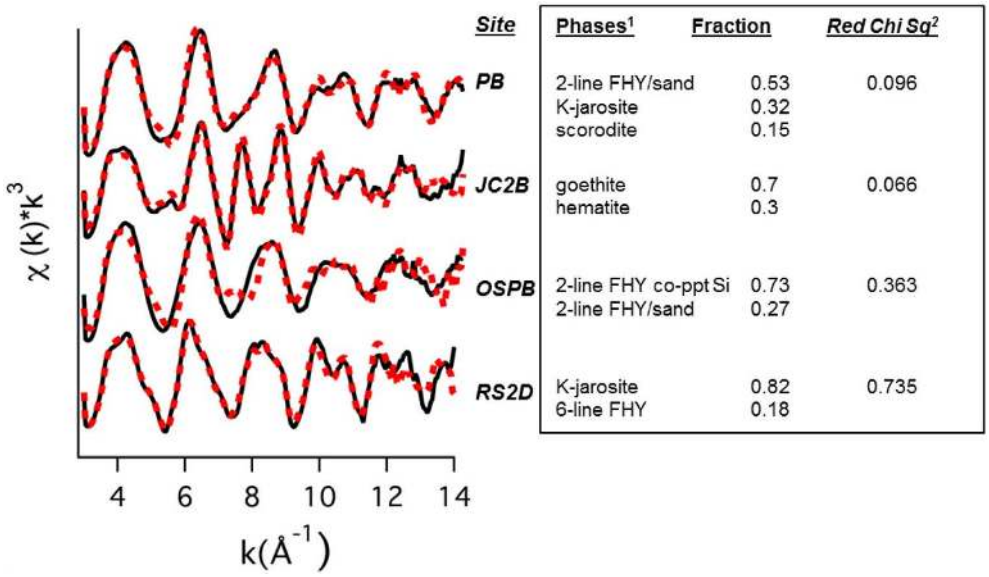

Site	Phases[1]	Fraction	Red Chi Sq[2]
PB	2-line FHY/sand	0.53	0.096
	K-jarosite	0.32	
	scorodite	0.15	
JC2B	goethite	0.7	0.066
	hematite	0.3	
OSPB	2-line FHY co-ppt Si	0.73	0.363
	2-line FHY/sand	0.27	
RS2D	K-jarosite	0.82	0.735
	6-line FHY	0.18	

FIGURE 5 | Least squares fits (dotted lines) to experimental k3 weighted Fe-EXAFS spectra (solid lines) obtained for solids from hot springs representing (bio)geochemical end-members. Predicted fractions of major solid phases (Fe standards 1) included in the fits are shown along with the reduced Chi square value.

filamentous-streamer communities dominated by *Hydrogenobaculum* sp. (NGB-OSP14). Gene sequences observed in OSP8 reveal extensive diversity from all orders of the Crenarchaeota (e.g., 13% *M. yellowstonensis* str. MK1) as well as novel groups (62%). In contrast, the filamentous "streamer" community (OSP14) archaeal clone library was dominated by *M. yellowstonensis* (67%), and less than 2% were related to novel archaeal groups (Thaumarchaeota as well as novel members of the Euryarchaeota). All bacterial clones ($n = 600$) amplified from these two sites in OSP Spring belong to the genus *Hydrogenobaculum*.

Deeper 16S rRNA gene sequence analysis using pyrotag sequencing (average nucleotide length = 180 bp) was also performed in several Fe-oxide microbial mats in NGB, including *OSP* Spring (OSPB, OSPC, OSPD), *Beowulf* Spring (BEE), and *Grendel* Spring (GRN_L). In addition, 16S rRNA sequences were obtained from assemblies of random shotgun metagenome sequence obtained from OSPB, OSPC, BED, and BEE. Given that several locations within OSP received random metagenome and pyrotag sequencing, comparison of phylogenetic signatures observed using the different methods was possible (**Table 2**), including reference to long-fragment 16S rRNA gene sequences from the above mentioned ribosomal panel obtained for OSP8 (which was sampled at same temperature as OSPB). Excellent agreement among three methods of assessing archaeal diversity was obtained for OSPB (**Table 2**) indicating that the higher temperature locations (i.e., 72–76˚C) in this spring are dominated by novel archaeal group I (NAG1, 50–60%), followed by *M. yellowstonensis* ∼12–20%), *Vulcanisaeta* spp. (∼10–15%), *Acidilobus* spp. (6–8%), a novel archaeal group II lineage (NAG2, ∼1–3%), and lower amounts of other novel archaeal groups (including Thaumarchaeota and Sulfolobales). Clustering of shorter pyrotag 16S sequences using long-fragment archaeal clone groups (e.g., those shown in **Figure 6**) from the same spring types (as opposed to only cultivated organisms with reference genomes) proved to be an excellent method of binning pyrotag sequences and estimates of percent abundance of the major taxonomic lineages in OSPB using pyrotag analysis are very close to estimates obtained from either long-fragment PCR analysis or binning of random metagenome sequence reads into the same phylogenetic groups (**Table 2**).

Comparison of pyrotag 16S rRNA gene sequence estimates with binning of random shotgun sequence reads from two additional sites (OSPC and D, 65 and 60˚C) also reveal excellent agreement between the two methods of obtaining semi-quantitative estimates of the distribution of archaea in Fe-oxide mats. Results from lower temperatures provide evidence for separation of NAG1 and NAG2 groups by temperature, where NAG2-like sequences increase in abundance as temperature decreases; at OSPD, NAG2-like sequences represent the dominant population (∼32%; **Table 2**). Other community members including *M. yellowstonensis* and NAG1 remain important at lower temperatures, and Sulfolobales strain MK5-like populations were slightly more abundant in OSPD.

Two additional Fe-oxide mat samples evaluated using pyrotag sequencing included locations within *Beowulf* and *Grendel* Springs (**Figure 8**). Although similar to end-member amorphous Fe-oxide mats of NGB including the OSP series discussed above, BEE and GRND_L reveal slightly different community types compared to OSP. Consistent populations observed compared to OSP include *M. yellowstonensis*, NAG1, NAG2, and novel Sulfolobales, however, GRND_L contained a significantly higher percentage of thaumarchaeal and novel Thermoplasmatales-like populations.

DESCRIPTION OF NOVEL ISOLATES

Four novel isolates were obtained from three different Fe-oxidizing springs in NGB and include members of the Sulfolobales

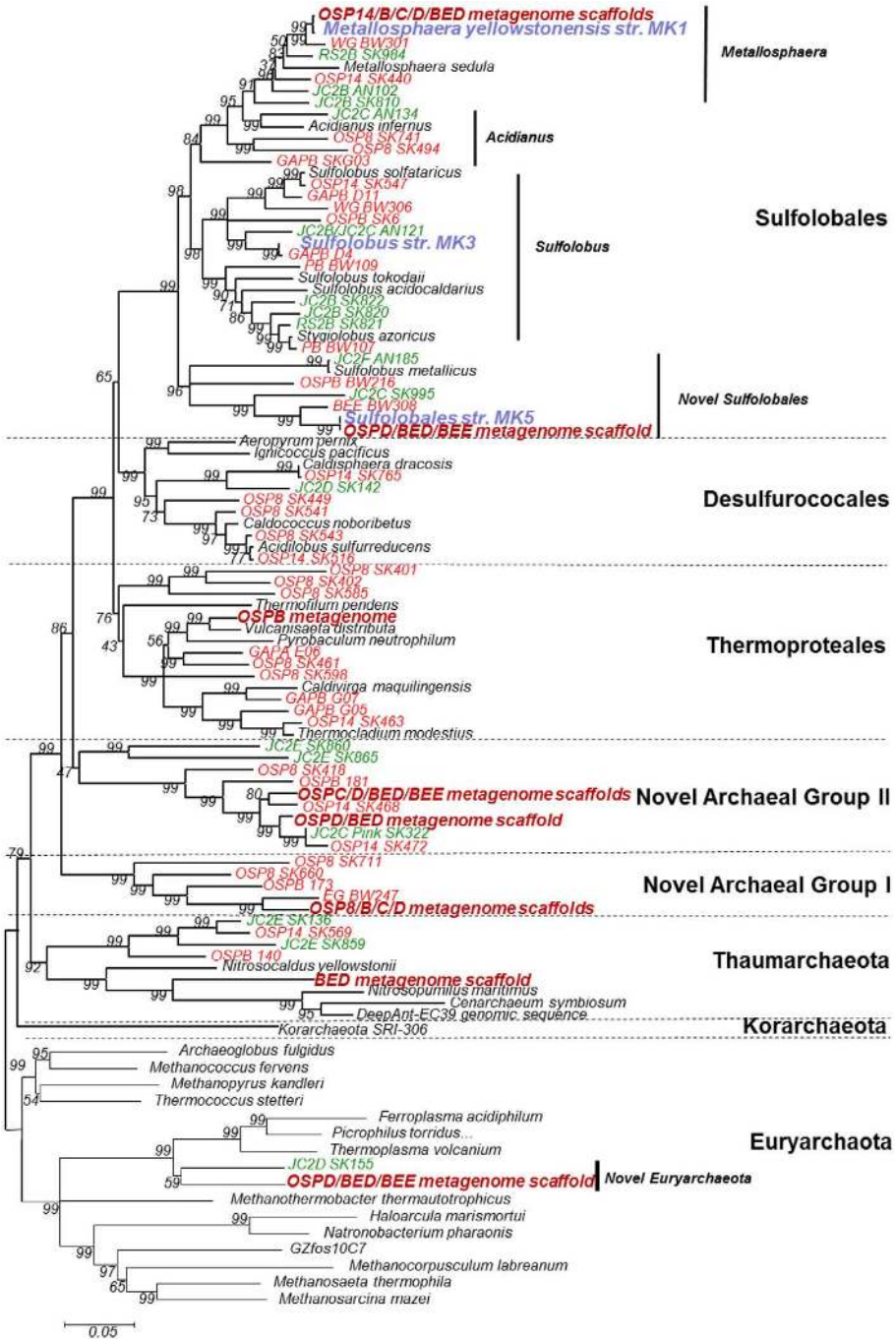

FIGURE 6 | Phylogenetic tree of archaeal 16S rRNA gene sequences (sequence length ∼1400 bp) observed across 19 different acidic iron mat samples from Yellowstone National Park (acid-sulfate-chloride springs are shown in red, acid-sulfate springs shown in green, isolates are highlighted in blue, and metagenome sequence entries are listed in dark red).

(*Sulfolobus* str. MK3, Sulfolobales str. MK5), Bacillales (*Sulfobacillus* str. MK2), and *Acidicaldus* str. MK6. A fifth isolate from *Beowulf* Spring, *M. yellowstonensis* str. MK1, has been described (Kozubal et al., 2008, 2011). The 16S rRNA gene sequences of strains MK2, MK3, and MK6 reveal similarity to previously described isolates ranging from 96 to 98%, and likely represent new species in the *Sulfobacillus*, *Sulfolobus*, and *Acidicaldus* genera, respectively (**Table 3**). However, Sulfolobales str. MK5 is only 88% similar to *Sulfolobus islandicus* (16S rRNA gene), and forms a completely new lineage within the current order Sulfolobales (**Figure 6**). Genome sequencing of strain MK5 is nearly complete and is currently represented as ∼2 Mb of assembled sequence on four scaffolds.

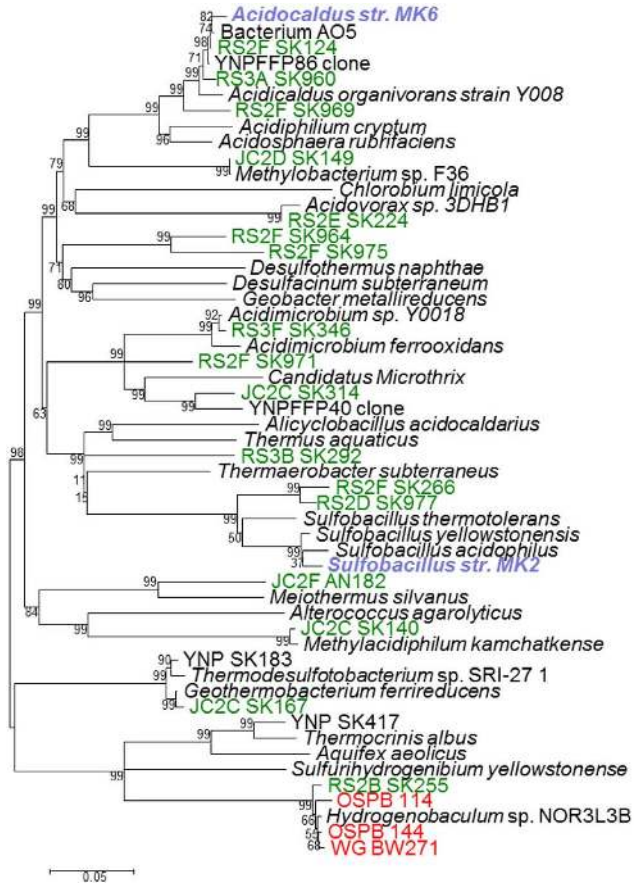

FIGURE 7 | Phylogenetic tree of bacterial 16S rRNA gene sequences (∼1400 bp) observed across 19 different acidic iron mats in Yellowstone National Park (acid-sulfate-chloride springs are shown in red, acid-sulfate springs shown in green, isolates are highlighted in blue, and metagenome sequence entries are listed in dark red).

All isolates were tested for growth using YE, Fe(II), S^0, pyrite, and solid media (**Table 3**). In addition, isolates were tested for their ability to fix carbon dioxide in carbon free media. *Sulfolobus* str. MK3 is capable of autotrophic growth and all isolates are capable of oxidizing Fe(II) except the *Acidicaldus* str. MK6. The Sulfolobales isolates (strains MK3 and MK5) are also capable of oxidizing pyrite (FeS_2). Moreover, strains MK5 and MK6 were shown to both reduce Fe(III) including amorphous Fe oxyhydroxides found in YNP Fe mats and a variety of ferric oxide minerals including hematite, ferrihydrite, and goethite. In fact, strain MK5 was shown to re-reduce Fe oxides (formed during aerobic growth) when grown under anoxic conditions using Gelrite® as a C and energy source. All strains were capable of utilizing complex carbon from yeast extract for heterotrophic growth, consequently, none are obligate autotrophs.

Both *Acidicaldus* str. MK6 and Sulfolobales str. MK5 grew on solid Gelrite® media as round white and cream colored colonies, respectively, whereas *Sulfobacillus* str. MK2 grew on 1.5% agar plates with 0.2% YE and 10 mM $FeSO_4$. Strain MK3 was not successfully grown on Gelrite® or agar plate media supplemented with 10 mM $FeSO_4$ and 0.2% YE and a variety of other plate media. The Sulfolobales isolates (strains MK3 and MK5) had higher temperature optimum (65–75˚C) than the two bacterial isolates (55–65˚C). All isolates grow optimally between pH 2.0 and 3.0; however, strains MK3 and MK5 exhibited slightly lower pH optima ranging from 2.0 to 2.5 (**Table 2**). Strain MK5 has the lowest pH range for growth and active cells were observed as low as 1.2. The Sulfolobales strains (MK3 and MK5) are ∼1 μm diameter cocci and/or irregular cocci, whereas both bacterial strains (*Sulfobacillus* str. MK2 and *Acidicaldus* str. MK6) are rod-shaped.

IRON OXIDATION AND REDUCTION RATES AND ANALYSIS OF CULTURE Fe SOLID PHASES

Iron oxidation rates were determined for Sulfolobales str. MK5 cultivated at 65˚C with 10 mM Fe(II) sorbed to sterile Fe-oxide mat (obtained from NGB-BE). Iron oxidation rates ranged from 15.7 ± 1.2 to 14.5 ± 2.9 fmol Fe(II) L^{-1} s^{-1}cell^{-1} at pH 1.5 and 2.5, respectively, for cultures grown autotrophically (without mixing/exposure to air only). Similar results were shown for *M. yellowstonensis* str. MK1 ranging from 7.4 ± 1.5 to 12.4 ± 3.1 fmol Fe(II) L^{-1} s^{-1}cell^{-1} at pH 3.2 and 2.5, respectively, reflecting slightly different pH optima between strains MK5 (this study) and *M. yellowstonensis* (Kozubal et al., 2008). The secondary phases formed during microbial Fe(II)-oxidation were determined for strain MK5 and *M. yellowstonensis* (not previously reported) grown on pyrite or Fe(II)-ferrihydrite (pyrite cultures shown in **Figure 9**) using both XRD and EXAFS. After 11 days of incubation under these growth conditions, hematite is the primary crystalline phase forming at the water-air interface (XRD analysis), whereas jarosite is found below the water surface. Least squares fitting of Fe-K-edge EXAFS spectra obtained on solid phases formed during microbial oxidation suggest mixed solid phases supported by XRD analyses (∼41% ferrihydrite, 24% jarosite, 16% goethite, and 12% hematite). XRD analysis of strain MK5 cultures revealed both goethite and jarosite in slurry samples from the bottom of the growth vessel (**Figure 9**). Consequently, Fe-oxidation products varied both with the isolate, location in the growth vessel, as well as across different spring compositions (**Table 1**; **Figure 4**). Under field conditions, jarosite was only observed at Rainbow and Joseph's Coat Springs (minor), where higher concentrations of "in channel" Fe(III), SO_4^{2-}, and K^+ all favor the formation of K-jarosite, despite lower saturation indices with respect to jarosite relative to the higher pH (3.1–3.5) systems of NGB (**Table 1**).

Evidence for a complete Fe redox cycle in thermophilic Fe mats was obtained from results of Fe(III)-reducing Sulfolobales strains MK5 and *Acidicaldus* strain MK6. Both isolates were shown to reduce Fe(III)-oxide solid phases, yielding soluble Fe(II). Iron reduction rates of 0.36 fmol Fe(III) L^{-1} s^{-1} cell^{-1} were determined in *Acidicaldus* str. MK6 cultures at pH 3.0 utilizing autoclaved Fe-mat as a source of ferric iron (**Figure 10**) and 10 mM glucose as the electron donor. Rates observed for MK5 were ∼0.5 fmol Fe(III) L^{-1} s^{-1} cell at pH 2.0.

RELEVANT GENES IN THE GENOME OF STRAIN MK5 AND SITE METAGENOMES

Preliminary genome analysis of strain MK5 shows that this organism contains syntenous sequences highly related to the *foxA-F* gene

Table 2 | Comparison of methods to determine phylogenetic distribution of archaeal lineages in Norris Geyser Basin OSP Spring.

Taxonomic lineage	Metagenome read binning (% total Archaea)	JGI ribosomal panel (% total Archaea)	16S rRNA pyro-tag sequences (% total Archaea)	Near full-length metagenome 16S rRNA sequences: Closest cultured relative or environmental sequence (% = nucleotide similarity; length bp)
OSPB				
NAG1	60.7	60.3	49.2	*Thermofilum* sp. 1505; 84% Koz183; 100% (1492)
Metallosphaera	11.7	16.1	21.3	*Metallosphaera yellowstonensis* str. MK1; 100% (1278)
Thermoproteales	15.2	9.9	12.6	*Vulcanisaeta distributa* IC-017; 98.4% SK409; 99.9% (1151)
Acidilobus	5.6	7.9	6.2	None
NAG2	1.1	3.4	2.5	*Staphylothermus* sp. 1633; 85.2% Koz169; 100% (1046)
Sulfolobales str. MK5	nd	0	2.4	None
Thaumarchaeota	nd	0	1.3	None
Other Archaea	5.8% unassigned contigs	2.4	3.7	None
OSPC				
NAG1	56.5		57.1	*Thermofilum* sp. 1505; 84% Clone Koz183; 100% (1334)
NAG2	28.7		17	*Staphylothermus* sp. 1633; 85.7% YNPFFA85; 99.6% (1354)
Metallosphaera	9.9		12	*Metallosphaera yellowstonensis* str. MK1; 99.6% (1354)
Thermoproteales	nd		9.2	None
Sulfolobales str. MK5	nd		1.5	None
Other archaea	5% unassigned contigs		3.1	None
OSPD				
NAG2	31.8		32	Seq1: *Staphylothermus hellenicus*;85.7% YNPFFA4 99.6% (1401) Seq2: *Staphylothermus* sp.1633; 85.7% YNPFFA85; 99.6% (1358)
NAG1	19.8		32	*Thermofilum* sp. 1505; 84% Koz183; 100% (1334)
Metallosphaera	19.2		21.2	*Metallosphaera yellowstonensis* str. MK1; 99.5% (1354)
Sulfolobales str. MK5	13.3		8.5	Sulfolobales str. MK5; 99.8% (1408)
Novel Euryarchaeota	8.1		0	*Aciduliprofundum* sp. EPR07-39; 86.5 BSLdp48 (1297)
Sulfolobus	7.8		4.3	None

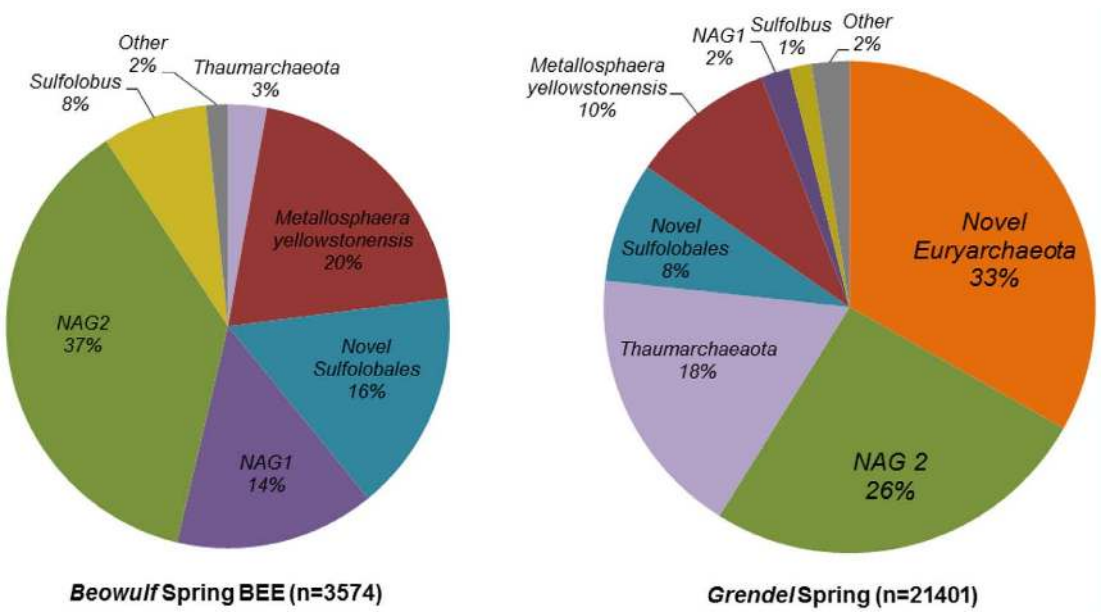

FIGURE 8 | Archaeal microbial community structure in two iron mat samples from Norris Geyser Basin presented as a percentage of total 16S rRNA gene pyrotag sequences that binned to different phylogenetic groups based on libraries of long-fragment sequences specific to these sites.

Table 3 | Novel isolates obtained from acid-sulfate-chloride (ASC) springs and characterization of cell morphology, pH optima, temperature optima, and growth on iron and sulfur substrates as electron donors or Fe(III) as an electron acceptor under anaerobic conditions.

Isolate	Cell morphology	Closest 16S rRNA relative (% similarity)	pH_{optima}	T_{optima} (°C)	Fix CO_2	Plate	H_2	Fe^{2+}	S^0	Pyrite	Fe^{3+}
Sulfolobus str. MK3	~1 μm cocci	*Sulfolobus* sp. T1 (96.6%)	2.0–2.5	75	+	−	−	+	+	+	−
Sulfolobales str. MK5	~1 μm cocci	*Sulfolobus islandicus* HVE10/4 (88%)	2.0–2.5	60–70	−	+	−	+	+	+	+
Sulfobacillus str. MK2	~3–5 μm rods	*Sulfobacillus acidophilus* TPY (98.3%)	2.0–3.0	55–58	−	+	−	+	+	+	−
Acidicaldus str. MK6	~1.2–1.5 μm rods up to 20–30 μm filaments	*Acidicaldus organivorans* str. Y008 (97.6%)	2.5–3.0	55–60	−	+	−	−	−	−	+

The ability to grow on solid media is also indicated. nd, Not determined.

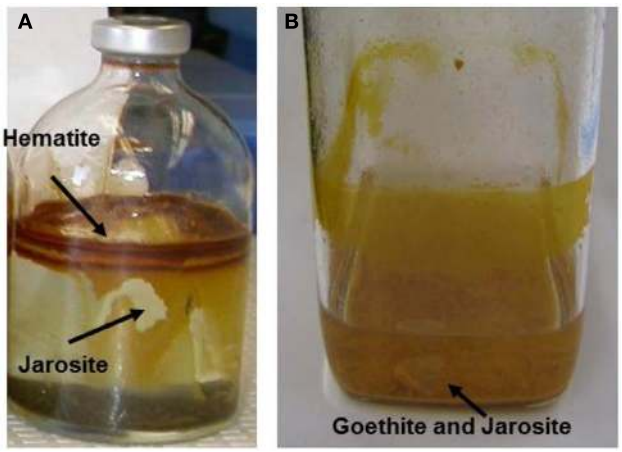

FIGURE 9 | Serum bottle culture of (A) *Metallosphaera yellowstonensis* str. MK1 and (B) Sulfolobales str. MK5 showing location of secondary phases sampled for solid phase analysis (11 days incubation, pyrite used as the electron donor).

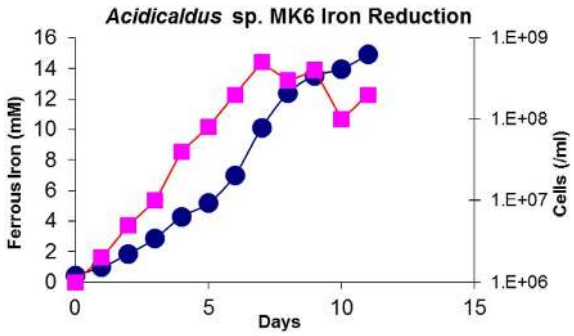

FIGURE 10 | Concentration of ferrous iron (mM) and cell counts (cells/mL) plotted as a function of time in anaerobic serum bottle cultures with *Acidicaldus* sp. strainMK6. Cultures were maintained at pH 3.0 with 10 mM glucose and 0.5 g autoclaved Fe-oxide mat from NGB-BED. Squares = cells/mL; circles = Fe(II)(mM).

cluster in *S. tokodaii* (Bathe and Norris, 2007). Like *S. tokodaii* and *S. metallicus*, strain MK5 has only one copy of *foxA* (the subunit I of the HCO) as compared to two copies in *M. sedula*, and three copies in *M. yellowstonensis* (Auernik et al., 2008; Kozubal et al., 2011). Strain MK5 also has a *cbsAB–soxL2N* gene operon, which has been identified as important in iron-oxidizing Sulfolobales (Kappler et al., 2005). Strain MK5 contains a gene encoding a sulfide quinone oxidoreductase (*sqr*) and a conserved *hdr* gene cluster important in elemental sulfur oxidation (Quatrini et al., 2009). Additionally, the strain has genes for a *tqoAD* thiosulfate oxidase directly upstream to the *cbsAB–soxL2N* gene operon. Strain MK5 does not contain genes for any of the known CO_2 fixation pathways (Berg et al., 2010). However the organism contains a number of genes encoding complex carbon degrading proteins including numerous cellulases, xylanases, and xenobiotic dioxygenases.

Metagenome analysis of NGB-BE and NGB-OSP yielded multiple copies of *fox* genes highly similar to those found in strain MK5 and *M. yellowstonensis*, suggesting these two organisms along with other Sulfolobales strains (e.g., *Sulfolobus* str. MK3) are the dominant populations responsible for Fe(II) oxidation via this mechanism. Genes related to cytochromes linked to Fe(II) oxidation in the well-characterized bacteria *Acidithiobacillus ferrooxidans* and *Leptospirillum* spp. were not found in the OSP and BE metagenomes (Jeans et al., 2008; Singer et al., 2008; Quatrini et al., 2009). Small blue copper proteins have also been associated with Fe(II) oxidation in *A. ferrooxidans* and the Euryarchaeota "*Ferroplasma acidarmanus*" (Dopson et al., 2005) and similar sequences were identified in the YNP metagenomes. However, most of these sequences are homologs of sulfocyanin (*soxE*) from *M. yellowstonensis* – and strain MK5-like species, which are more likely involved in the SoxM-like terminal oxidase complex specific for heterotrophy, and not involved in Fe(II) oxidation (Kozubal et al., 2011).

DISCUSSION

Ferric iron mats of NGB, Joseph's Coat, and Rainbow Springs in YNP exhibit considerable microbial diversity as shown by the extensive compilation of phylogenetic data including 1500 full-length 16S rRNA gene sequences, over ~40,000 pyrotag sequences and five shotgun metagenome sequences from BED, BEE, OSPB, OSPC, and OSPD. The Sulfolobales are important in all 18 spring

sites as indicated by the high percentage of 16S rRNA sequences and binning of metagenome sequence reads. *M. yellowstonensis* str. MK1-like 16S rRNA gene sequences are highly dominant in most sampling points particularly in Joseph's Coat and Rainbow Springs between 60 and 75°C. In addition, metagenome data strongly suggest that *M. yellowstonensis*-like populations are important in NGB-BE and NGB-OSP Springs as evidenced by the number of total reads binning to the *M. yellowstonensis* genome (Inskeep et al., 2010). Detailed community analysis of *M. yellowstonensis* related species along with expression of *fox* genes *in situ* are discussed in more detail elsewhere (Kozubal et al., 2011). Novel Sulfolobales-like MK5-like populations also contribute a high percentage of metagenome reads and 16S rRNA gene sequences, but at slightly lower temperatures (e.g., OSPC and OSPD).

Sequences from members of the Desulfurococcales, Thermoproteales, and novel archaeal lineages are also important in YNP ferric iron mats. In addition, sites below 65°C are characterized by highly divergent 16S rRNA bacterial gene sequences especially at sites RS2F and RS3B. Many of these bacterial sequences are less than 90% similar to cultivated relatives and represent three new taxonomic branches at the order level and higher (**Figure 7**). Above 70°C, bacterial gene sequences are completely dominated by *Hydrogenobaculum* spp. and detailed sequence analysis of NG-OSP and RS2 reveal two distinct sub-clades.

The microbial community structure of acidic iron mats is likely driven by the flux of O_2 required to drive Fe(II) oxidation, as well as the presence of other reduced inorganic electron donors available for growth. However, temperature and pH are also important parameters controlling community structure. For instance, sequences related to *Acidilobus* spp., *Stygiolobus azoricus*, and Thermoproteales spp. (i.e., *Vulcanisaeta distributa*) dominate at higher temperatures, consistent with the range observed for cultivated relatives. Moreover, bacteria such as *Sulfobacillus* and *Acidicaldus* spp. thrive at lower temperatures. *M. yellowstonensis* was found to be prevalent in all sites, and the relative importance of novel populations such as NAG1, NAG2, Thaumarchaeota and Euryarchaeota varies across sites. However, the primary populations involved directly in Fe cycling appear to be aerobic organisms that use the Fox terminal oxidase complex consistent with genome, metagenome, and prior mRNA expression analysis.

The five isolates discussed in this study are highly relevant to our understanding of geomicrobiology and microbial ecology of acidic geothermal ferric iron mats of YNP. All isolates are capable of oxidizing iron and strains MK5 and MK6 are also capable of ferric iron reduction under anaerobic conditions. *M. yellowstonensis* and *Sulfolobus* str. MK3 are capable of autotrophic growth and are likely important primary producers *in situ* linking CO_2 fixation directly with Fe(II) oxidation. These organisms may be a significant source of carbon for other microorganisms such as *Acidicaldus* str. MK6, which may need this carbon source for anaerobic growth on Fe(III). Therefore, the Sulfolobales isolates offer an excellent opportunity to understand mechanisms of CO_2 fixation in model natural systems. Uncharacterized archaeal and bacterial populations in ferric oxide mats may also be linked to other electron donors besides Fe(II) (**Table 1**). For instance, *Methylacidiphilum*-like sequences are found in JC2F and RS3A at 70 and 29% of bacterial sequences, respectively, and may take advantage of the relatively high CH_4 concentrations (2.2 and 3.5 μM) compared to other spring locations. These organisms remain a high priority for isolation.

Analysis of ferric solid phases on serum bottle cultures link observed biomineralized phases found in the springs to cultured organisms. Spring geochemistry [i.e., sulfate and Fe(III) concentrations, pH, presence of arsenate] plays an important role in the formation of mineral phases. However, populations highly similar to strains MK1 and MK5 contribute directly to the observed oxidation of Fe(II) in YNP ferric iron mats and especially MK1-like populations in RS2 and JC2 above 65°C (Kozubal et al., 2008). In culture, *M. yellowstonensis* forms hematite and jarosite on serum bottle surfaces and XRD analysis of strain MK5 identified jarosite and goethite as a slurry on the vessel bottom (**Figure 9**). The different ferric iron phases found in cultures stress that different microbial processes (both "biologically controlled" and "biologically induced") are important in determining the iron phases formed. Moreover, different solution conditions contribute to variation in solid phases observed across field sites.

Strains MK1 and MK5 oxidize Fe(II) at rates similar to those observed in other archaeal species under similar culture conditions (Nemati and Harrison, 2000; Kauppi et al., 2001). Both strains exhibit faster rates of Fe(II)-oxidation at lower pH, which is consistent with observations of other acidophilic Fe(II)-oxidizing microorganisms. The fixation of CO_2 under culture conditions was observed only for strain MK1. In fact, genes for any of the six known CO_2 fixation pathways were not found in strain MK5 (Berg et al., 2010), which is unique compared to other Sulfolobales (all reference Sulfolobales genomes contain genes for the 3-hydroxypropionate/4-hydroxybutyrate pathway). However, strain MK5 has genes that encode for a wide range of proteins known to be involved in the degradation of complex carbon sources. Consequently, these results suggest strain MK1 is a dominant primary producer that links CO_2 fixation to Fe(II) oxidation, whereas strain MK5 is a mixotroph linking Fe(II) oxidation to utilization of complex carbon. Strain MK5 is also capable of Fe(III) reduction by an unknown mechanism and may, alternatively, define its niche *in situ* as an anaerobic complex carbon degrader linked to Fe(III) respiration. Elucidating the mechanism of Fe(III) reduction in strain MK5 will be an important future priority for understanding iron cycling in these systems.

The oxidation of Fe(II) in high-temperature environments may have also been important in Earth's early evolutionary history (>2–3 Ga). The biomineralization of ferric iron phases (e.g., jarosite) and the evolution of key metabolic processes such as aerobic respiration in high-temperature Fe mats has implications for the fields of paleobiology and exobiology, as well as microbiology. The findings presented in this study represent the most detailed analysis of geothermal acidic ferric iron mats reported to date, and will be invaluable for future comparative studies to similar undescribed environments.

ACKNOWLEDGMENTS

This work was supported by the National Science Foundation Microbial Observatory Program (MCB-0132022), the National Aeronautic and Space Administration (NASA) via funds provided to the Thermal Biology Institute at Montana State University

(Project Numbers NAG5-8807, NNG04GR46G), the Stanford Synchrotron Radiation Laboratory (SSRL), the DOE-Pacific Northwest National Laboratory (Subcontract 112443), the NSF IGERT Program (0654336), and the Montana Agricultural Experiment Station (Project 911300). The authors appreciate assistance from, S. Korf, W. P. Taylor, A. Nagy, and G. Ackerman for field work, geochemical analyses, sample collection, and 16S rRNA sequencing, and Drs. Scott Fendorf, S. Webb, and J. Bargar for assistance in collecting and analyzing Fe-edge XANES and EXAFS spectra at SSRL. The authors also appreciate C. Hendrix and T. Olliff for permitting this work in Yellowstone National Park (Permit YELL-2004-2007-SCI-5068). The work conducted by the U.S. Department of Energy Joint Genome Institute is supported by the Office of Science of the U.S. Department of Energy under Contract No. DE-AC02-05CH11231. Portions of this research were carried out at the Stanford Synchrotron Radiation Lightsource (SSRL), a national user facility operated by Stanford University on behalf of the U.S. Department of Energy, Office of Basic Energy Sciences. Thomas Borch was supported by a NSF CAREER Award (EAR 0847683).

REFERENCES

Auernik, K. S., Maezato, Y., Blum, P. H., and Kelly, R. M. (2008). The genome sequence of the metal-mobilizing, extremely thermoacidophilic archaeon *Metallosphaera sedula* provides insights into bioleaching-associated metabolism. *Appl. Environ. Microbiol.* 3, 682–692.

Baker, B. J., and Banfield, J. F. (2003). Microbial communities in acid mine drainage. *FEMS Microbiol. Ecol.* 44, 139–152.

Bathe, S., and Norris, P. R. (2007). Ferrous iron- and sulfur-induced genes in *Sulfolobus metallicus*. *Appl. Environ. Microbiol.* 8, 2491–2497.

Beam J. P., Bernstein, H. C., Kozubal, M., Carlson, R. P., and Inskeep, W. P. (2011). "Distribution and activity of iron-oxidizing microorganisms in acidic geothermal environments," in *Goldschmidt Conference, August 15–19*, Vol. 75 (Prague: Mineralogical Magazine), 503.

Berg, I. A., Kockelkorn, D., Ramos-Vera, W. H., Say, R. F., Zarzycki, J., Hügler, M., Alber, B. E., and Fuchs, G. (2010). Autotrophic carbon fixation in archaea. *Nat. Rev. Microbiol.* 8, 447–460.

Blake, R., and Johnson, D. B. (2000). "Phylogenetic and biochemical diversity among acidophilic bacteria that respire on iron," in *Environmental Microbe–Metal Interactions*, ed. D. R. Lovley (Washington: ASM Press), 53–78.

Dopson, M., Baker-Austin, C., and Bond, P. L. (2005). Analysis of differential protein expression during growth states of *Ferroplasma* strains and insights into electron transport for iron oxidation. *Microbiology* 151, 4127–4137.

Edwards, K. J., Goebel, B. M., Rodgers, T. M., Schrenk, M. O., Gihring, T. M., Cardona, M. M., Hu, B., McGuire, M. M., Hamers, R. J., Pace, N. R., and Banfield, J. F. (1999). Geomicrobiology of pyrite (FeS2) dissolution: case study at Iron Mountain, California. *Geomicrobiol. J.* 16, 155–179.

Engelbrektson, A., Kunin, V., Wrighton, K. C., Zvenigorodsky, N., Chen, F., Ochman, H., and Hugenholtz, P. (2010). Experimental factors affecting PCR-based estimates of microbial species richness and evenness. *ISME J* 5, 642–647.

Hallberg, K. B., and Johnson, D. B. (2001). Biodiversity of acidophilic prokaryotes. *Adv. Appl. Microbiol.* 49, 37–84.

Inskeep, W. P., Ackerman, G. G., Taylor, W. P., Kozubal, M., Korf, S., and Macur, R. E. (2005). On the energetics of chemolithotrophy in nonequilibrium systems: case studies of geothermal springs in Yellowstone National Park. *Geobiology* 3, 297–320.

Inskeep, W. P., Macur, R. E., Harrison, G., Bostick, B. C., and Fendorf, S. (2004). Biomineralization of As(V)-hydrous ferric oxyhydroxide in microbial mats of an acid-sulfate-chloride geothermal spring, Yellowstone National Park. *Geochim. Cosmochim. Acta* 68, 3141–3155.

Inskeep, W. P., Rusch, D., Jay, Z., Herrgard, M. J., Kozubal, M. A., Richardson, T. H., Macur, R. E., Hamamura, N., Fouke, B., Reysenbach, A. L., Roberto, F., Young, M., Jennings, R., Schwartz, A., Korf, S., Boyd, E., Badger, J., Bateson, M., Geesey, G., Mathur, E., and Frazier, M. (2010). Metagenomes from high-temperature chemotrophic systems reveal geochemical controls on microbial community structure and function. *PLoS ONE* 5, e9773. doi:10.1371/journal.pone.0009773

Itoh, Y. H., Kurosawa, N., Uda, I., Sugai, A., Tanoue, S., Itoh, T., Horiuchi, T., and Itoh, T. (2001). *Metallosphaera sedula* TA-2, a calditoglycerocaldarchaeol deletion strain of a thermoacidophilic archaeon. *Extremophiles* 5, 241–245.

Jackson, C. R., Langner, H. W., Donahoe-Christiansen, J., Inskeep, W. P., and McDermott, T. R. (2001). Molecular analysis of microbial community structure in an arsenite-oxidizing acidic thermal spring. *Environ. Microbiol.* 3, 532–542.

Jeans, C., Singer, S. W., Chan, C. S., Verberkmoes, N. C., Shah, M., Hettich, R. L., Banfield, J. F., and Thelen, M. P. (2008). Cytochrome 572 is a conspicuous membrane protein with iron oxidation activity purified directly from a natural acidophilic microbial community. *ISME J* 2, 542–550.

Johnson, D. B., and Hallberg, K. B. (2009). Carbon, iron and sulfur metabolism in acidophilic micro-organisms. *Adv. Microb. Physiol.* 54, 202–256.

Johnson, D. B., Okibe, N., and Roberto, F. F. (2003). Novel thermo-acidophilic bacteria isolated from geothermal sites in Yellowstone National Park: physiological and phylogenetic characteristics. *Arch. Microbiol.* 180, 60–68.

Johnson, D. B., Stallwood, B., Kimura, S., and Hallberg, K. B. (2006). Isolation and characterization of *Acidicaldus organivorus*, gen. nov., sp. nov.: a novel sulfur-oxidizing, ferric iron-reducing thermo-acidophilic heterotrophic *Proteobacterium*. *Arch. Microbiol.* 185, 212–221.

Kappler, A., and Straub, K. L. (2005). Geomicrobiological cycling of iron. *Rev. Mineral. Geochem.* 59, 85–108.

Kappler, U., Sly, L. I., and McEwan, A. G. (2005). Respiratory gene clusters of *Metallosphaera sedula* – differential expression and transcriptional organization. *Microbiology* 151, 35–43.

Kauppi, P. H., Hautakangas, H. J., and Puhakka, J. A. (2001). High rate iron oxidation in fluidized-bed bioreactors. *Proc. Int. Biohydrometal. Symp.* 2001, 385–392

Konhauser, K. O. (1998). Diversity of bacterial iron mineralization. *Earth Sci. Rev.* 43, 91–121.

Konhauser, K. O. (2007). *Introduction to Geomicrobiology*. Oxford: Blackwell Science, 425.

Kozubal, M., Macur, R. E., Korf, S., Taylor, W. P., Ackerman, G. G., Nagy, A., and Inskeep, W. P. (2008). Isolation and distribution of a novel iron-oxidizing crenarchaeon from acidic geothermal springs in Yellowstone National Park. *Appl. Environ. Microbiol.* 74, 942–949.

Kozubal, M. A., Dlakic, M., Macur, R. E., and Inskeep, W. P. (2011). Terminal oxidase diversity and function in "*Metallosphaera yellowstonensis*": gene expression and protein modeling suggest mechanisms of Fe(II) oxidation in the sulfolobales. *Appl. Environ. Microbiol.* 77, 1844–1853.

Macur, R. E., Langner, H. W., Kocar, B. D., and Inskeep, W. P. (2004). Linking geochemical processes with microbial community analysis: successional dynamics in an arsenic-rich, acid-sulfate-chloride geothermal spring. *Geobiology* 2, 163–177.

Nemati, M., and Harrison, S. T. L. (2000). A Comparative Study on thermophilic and mesophilic biooxidation of ferrous iron. *Miner. Eng.* 13, 19–24.

Nordstrom, D. K., and Southam, G. (1997). Geomicrobiology of sulfide mineral oxidation. *Rev. Mineral. Geochem.* 35, 361–390.

Quatrini, R., Appia-Ayme, C., Denis, Y., Jedlicki, E., Holmes, D. S., and Bonnefoy, V. (2009). Extending the models for iron and sulfur oxidation in the extreme acidophile *Acidithiobacillus ferrooxidans*. *BMC Genomics* 10, 394. doi:10.1186/1471-2164-10-394

Rohwerder, T., Gehrke, T., Kinzler, K., and Sand, W. (2003). Bioleaching review part A: progress in bioleaching: fundamentals and mechanisms of bacterial metal sulfide oxidation. *Appl. Microbiol. Biotechnol.* 63, 239–248.

Singer, P. C., and Stumm, M. W. (1970). Acid mine drainage: the rate determining step. *Science* 167, 1121–1123.

Singer, S. W., Chan, C. S., Zemla, A., VerBerkmoes, N. C. M., Hwang, M., Hettich, R. L., Banfield, J. F., and Thelen, M. P. (2008). Characterization of cytochrome 579, an

unusual cytochrome isolated from an iron-oxidizing microbial community. *Appl. Environ. Microbiol.* 74, 4454–4456.

Tamura, K., Peterson, D., Peterson, N., Stecher, G., Nei, M., and Kumar, S. (2011). MEGA5: molecular evolutionary genetics analysis using maximum likelihood, evolutionary distance, and maximum parsimony methods. *Mol. Biol. Evol.* 28, 2731–2739.

To, T. B., Nordstrom, D. K., Cunningham, K. M., Ball, J. W., and McClesky, R. B. (1999). New method for the direct determination of dissolved Fe(III) concentration in acid mine waters. *Environ. Sci. Technol.* 33, 807–813.

Webb, S. (2011). *Sixpack v.0.68; Stanford Synchrotron Radiation Lightsource.* Menlo Park: SLAC National Accelerator Laboratory.

Conflict of Interest Statement: The authors declare that the research was conducted in the absence of any commercial or financial relationships that could be construed as a potential conflict of interest.

Received: 03 November 2011; accepted: 05 March 2012; published online: 26 March 2012.

*Citation: Kozubal MA, Macur RE, Jay ZJ, Beam JP, Malfatti SA, Tringe SG, Kocar BD, Borch T and Inskeep WP (2012) Microbial iron cycling in acidic geothermal springs of Yellowstone National Park: integrating molecular surveys, geochemical processes, and isolation of novel Fe-active microorganisms. Front. Microbio. **3**:109. doi: 10.3389/fmicb.2012.00109*

This article was submitted to Frontiers in Microbiological Chemistry, a specialty of Frontiers in Microbiology.